

## $\gamma$ - $\gamma$ Angular Correlation Measurements of Thermal-Neutron Capture $\gamma$ Rays in Magnesium, Silicon, Phosphorus, and Sulfur

G. MANNING\* AND G. A. BARTHOLOMEW  
Atomic Energy of Canada Limited, Chalk River, Ontario, Canada

(Received February 16, 1959)

A description is given of an angular correlation apparatus, using two NaI (Tl) scintillation spectrometers, which has been used to study cascades of  $\gamma$  radiation following thermal neutron capture. The elements studied were magnesium, silicon, phosphorus, and sulfur. The following new spin assignments were made: the 4.93-Mev level of  $\text{Si}^{29}$ ,  $\frac{3}{2}$ ; 6.38-Mev level of  $\text{Si}^{29}$ ,  $\frac{1}{2}$ ; 1.15-Mev level of  $\text{P}^{32}$ , 1; and 3.26-Mev level of  $\text{P}^{32}$ , 2. In addition, the spins of the 3.41-Mev level of  $\text{Mg}^{25}$  and the 3.22-Mev level of  $\text{S}^{33}$  have been confirmed to be  $\frac{3}{2}$ . Other aspects of the decay schemes are discussed.

### I. INTRODUCTION

MEASUREMENT of the angular correlation between cascade  $\gamma$  rays following either  $\beta$  decay or charged particle reactions is a common technique of nuclear spectroscopy. Such measurements, under favorable circumstances, may give information concerning the spins of nuclear levels and sometimes may lead to the determination of the magnitude and sign of the multipole mixture parameter of one of the  $\gamma$  rays. The technique is also applicable to the study of  $\gamma$ - $\gamma$  cascades following neutron capture but to date only limited use has been made of it in this field. Recksiedler and Hamermesh,<sup>1</sup> Segel,<sup>2</sup> Trumpy<sup>3</sup> and Kennett *et al.*<sup>4</sup> have made coincidence measurements between cascade  $\gamma$  rays following neutron capture but only Trumpy<sup>3</sup> has reported angular correlations between these radiations.

### II. APPARATUS

A diagram of the apparatus used for the present measurements is shown in Fig. 1. A neutron beam from an experimental hole in the Chalk River NRX reactor was diffracted from a lead crystal and used to bombard the target to be studied, which was placed inside a shielded enclosure. The cascade  $\gamma$  radiation from the target was detected by two scintillation spectrometers used in a coincidence arrangement. One detector was held stationary and the other could be rotated about the axis of the target over the range of angles from 90° to approximately 220° with respect to the fixed detector.

The neutron beam was diffracted in order to remove the epithermal neutrons present in the initial beam. The beam was diffracted from the (111) planes of a 1½-in. thick lead crystal at a Bragg angle of 12.5 degrees. This angle was chosen empirically to maximize the  $\gamma$ -ray yield from the target. The diffracted neutrons had a

wavelength of 1.2 Å corresponding to an energy of 0.054 eV. The neutron flux at the target position was approximately  $6 \times 10^5$  neutrons  $\text{cm}^{-2} \text{sec}^{-1}$  and the beam diameter was 1.6 in. The targets used were 1 in. or less in diameter, which tended to ensure that they were uniformly irradiated. When powder targets were used the powder was contained in a Lucite capsule with  $\frac{3}{16}$ -inch thick walls.

The thermal neutrons scattered from the target were absorbed by a cylinder of  $\text{Li}^6$  metal approximately  $\frac{1}{8}$ -inch thick placed around the target, Fig. 1. The  $\text{Li}^6$  metal was protected from moisture by a thin stainless steel cylinder on the outside and by a Lucite cylinder<sup>5</sup> on the inside. The  $\text{Li}^6$  metal was pressure-molded in position between the protective walls with the aid of a mechanical press. The  $\text{Li}^6$  screen attenuated the thermal neutrons by a factor of about  $10^6$  but was practically transparent to the majority of  $\gamma$  rays studied. No difficulty was found in working with  $\gamma$  rays with energies as low as 80 keV.

The scintillation spectrometers were four-inch diameter, six-inch long NaI (Tl) crystals mounted on five-inch diameter 6364 Du Mont photomultiplier tubes. The crystals were encased in lead shielding approximately 1 inch thick with conical lead collimators mounted between the target and the crystals; see Fig. 1. This shielding is effective in reducing the counting rate caused by various spurious coincidence effects. Among these unwanted events are those in which one of the two coincident  $\gamma$  rays is detected by one crystal while the other strikes the walls of the enclosure and produces secondary radiation which is detected by the other crystal. Another spurious event involves the detection in one crystal of annihilation radiation or Compton secondary radiation produced by the interaction of one  $\gamma$  ray in the other crystal. For events of the latter type the lead shielding encasing the crystals becomes almost ineffective as the angle between the detectors approaches 180°. The collimators defined an entrance aperture 3 inches in diameter at the face of each crystal.

<sup>5</sup> The 2.23-Mev  $\gamma$ -ray following capture in the hydrogen of the Lucite cylinder and target holder proved to be a useful calibration line which accompanied all spectra studied.

\* Present address: Norman Bridge Laboratory of Physics, California Institute of Technology, Pasadena, California.

<sup>1</sup> A. L. Recksiedler and B. Hamermesh, *Phys. Rev.* **96**, 109 (1954).

<sup>2</sup> R. E. Segel, *Bull. Am. Phys. Soc. Ser. II*, **2**, 230 (1957).

<sup>3</sup> G. Trumpy, JENER (Joint Establ. Nuclear Energy Research), Pubs. No. 13 (1957).

<sup>4</sup> Kennett, Bollinger, and Carpenter, *Phys. Rev. Letters* **1**, 76 (1958).

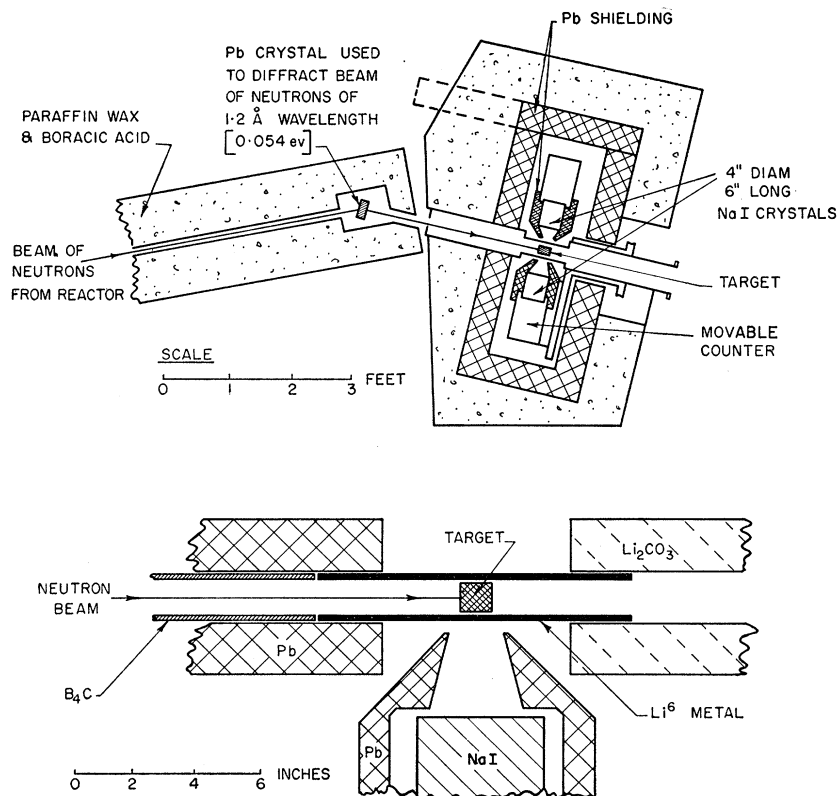


FIG. 1. Apparatus used to study angular correlations between cascade  $\gamma$  radiation following thermal neutron capture. The upper part of the figure shows the general arrangement of counters and shielding, the lower part shows some details of the shielding close to the counters.

The crystal faces were situated 4 inches from the target axis so that the solid angle subtended by each detector at the center of the target was 3.5% of  $4\pi$ . Both photomultiplier tubes were surrounded by  $\mu$ -metal shields. The energy resolution of the spectrometers depended upon the energy of the  $\gamma$  rays detected and was about 12%<sup>6</sup> for energies near 0.7 Mev and about 7% near 2 Mev. The detectors were shielded from general pile background by a lead box with 5-in. thick walls surrounded by a neutron shield consisting of a mixture of paraffin wax and boracic acid, some 10 inches thick.

To take coincidence spectra, pulses from the movable detector in coincidence with a narrow pulse-height range in the stationary detector were recorded in a 100-channel pulse-height analyzer.<sup>7</sup> A block diagram of the electronics used is given in Fig. 2. The coincidence arrangement is a typical fast-slow system (see Bell, Graham, and Petch<sup>8,9</sup>) with a resolving time,  $\tau$ , of  $2 \times 10^{-8}$  sec.

The apparatus was designed so that it could be

<sup>6</sup> Full width at half peak intensity of the full energy peak.

<sup>7</sup> F. S. Goulding, Natl. Acad. Sci.—Natl. Research Council, Publ. No. 467, 86 (1957).

<sup>8</sup> Bell, Graham, and Petch, Can. J. Phys. **30**, 35 (1952).

<sup>9</sup> The present circuit differed from that described in the reference mainly in the treatment of the pulses between the photomultiplier and the fast coincidence circuit. Before entering the coincidence circuit the pulses were amplified in three distributed amplifiers in series with a total voltage gain of 600 and a band width of 100 Mc/sec. The pulses were clipped at  $10^{-7}$  sec with a shorted cable at the output of the first distributed amplifier.

operated automatically. The operation was controlled by a programming circuit which made it possible to preselect any sequence of as many as 15 positions for the movable counter and the time for counting at that position. The 15 positions were chosen so that the angle between the counters could be changed in units of 0.1 in  $\cos^2\theta$ , where  $\theta$  is the angle between the counters. At the end of each counting time the following information was recorded by an electric typewriter: the angle between the counters, the counting time at that angle, the spectrum in the 100-channel pulse-height analyzer and the number accumulated in a scaler. The scaler was in general used to record the number of counts within the narrow pulse height range accepted from the stationary detector. The spectrum from the 100-channel pulse-height analyzer was simultaneously punched on eight-channel paper tape. The normal method of programming the equipment was to repeat observations taken at the angles selected in cyclic order, counting for a fixed time at each angle. A typical time was 30 minutes. The paper tape was read into a digital computer at the end of each complete run and the spectra for each angle were summed channel by channel. The computer printed a 100-channel spectrum for each angle, summed over the many observations made at that angle. In this way only one final spectrum was analyzed at each angle but random fluctuations such as changes in efficiency of the

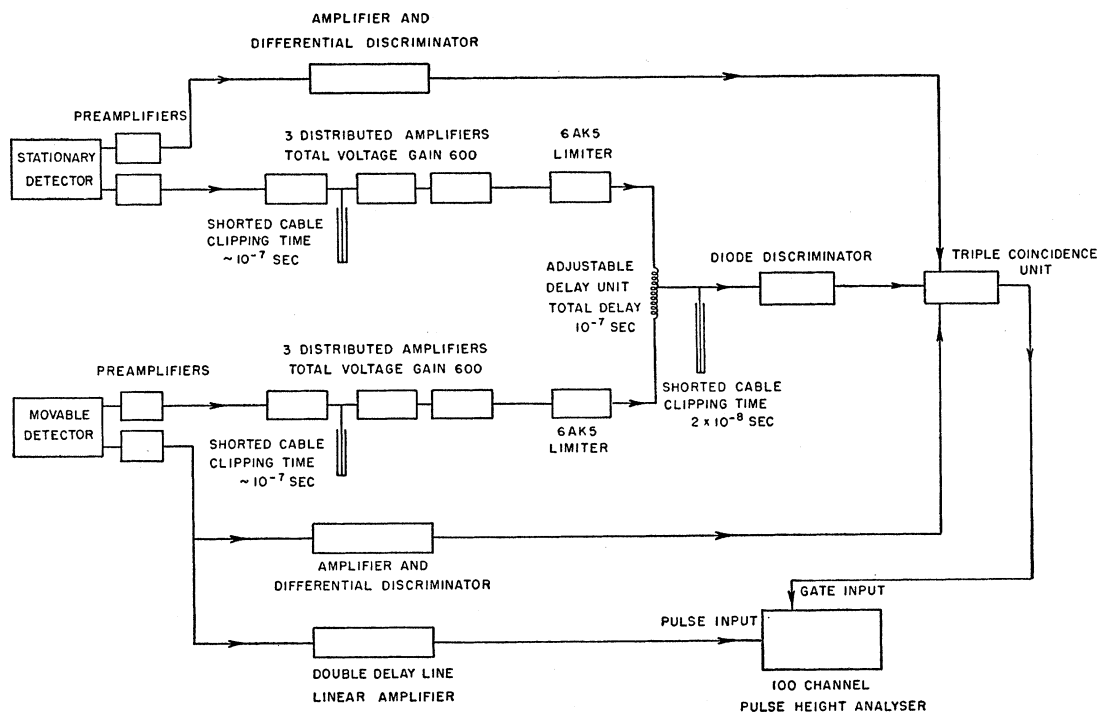


FIG. 2. Block diagram of electronic apparatus. The apparatus is a conventional fast-slow coincidence arrangement with a resolving time,  $\tau$ , of  $2 \times 10^{-8}$  sec.

coincidence system, small variations in pile power,<sup>10</sup> small changes in the energy calibration of the detectors, etc., were averaged out.

For targets of 1-in. diameter which were black to thermal neutrons, source strengths of about  $10^7$   $\gamma$  rays per second could be produced. In general this was more than sufficient and source strengths of  $10^6$   $\gamma$  rays per second, or less, were normally used. The neutron flux at the target position was sufficiently high to allow materials with cross sections as low as 30 mb to be studied without difficulty.

In the absence of a sample, the background counting rate above a lower bias equivalent to an energy loss of 100 kev in the crystals was about 6000 per sec. The majority of this counting rate was due to activity built up in the sodium iodide crystals by neutron bombardment. The neutrons were present largely because, due to lack of space, the neutron shielding surrounding the lead box was not complete. However, this high background rate was of little trouble in coincidence measurements since the coincidence counting rate obtained without a target and with typical energy ranges accepted by the detectors was less than one per minute. This rate is negligible compared to the counting rates used in the experiments described below.

<sup>10</sup> The pile power was monitored and if changes greater than  $\pm 2\%$  occurred during an experiment the results were not accepted.

### III. GEOMETRIC CORRECTIONS AND TEST EXPERIMENTS

Spurious asymmetries in the counting rate of the rotating detector as a function of angle may be caused by displacement of the target, or the neutron beam, from the axis of rotation, or by small changes in magnetic field which might affect the performance of the moving photomultiplier. Careful tests made using various  $\gamma$ -ray sources showed that the change in counting rate due to these effects was less than 0.5%. As a further test, the correlation function between the 1.28-Mev and 0.51-Mev annihilation radiation from a  $\text{Na}^{22}$  source was measured. The correlation should be isotropic in the absence of the effects mentioned above. A least-squares fit to the observations made at 6 angles between  $90^\circ$  and  $180^\circ$  gave

$$W(\theta) = 1 + (0.01 \pm 0.02)P_2(\cos\theta).^{11}$$

In general an observed correlation function must be corrected for the finite angle of acceptance of the detectors and the finite target size. Feingold and Frankel<sup>12</sup> calculate these corrections for the case of a long thin source on the axis of rotation of the movable detector. For a target length of one inch and the geometry used in the measurements described below (*viz.*, a detector 3 inches in diameter 4 inches from the axis of rotation),

<sup>11</sup>  $P_2(\cos\theta)$  is the second order Legendre Polynomial.

<sup>12</sup> A. M. Feingold and S. Frankel, Phys. Rev. **97**, 1025 (1955).

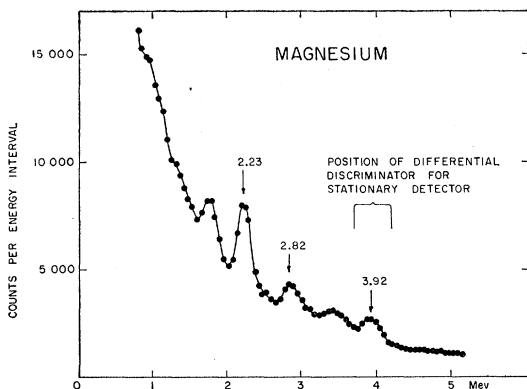


FIG. 3. Typical direct pulse-height spectrum observed with one of the detectors using a magnesium target. The background spectrum has not been subtracted. The 2.23-Mev  $\gamma$  ray results from neutron capture in the hydrogen in the Lucite target support. The range of pulses accepted for the coincidence measurements is shown.

these corrections change a distribution of the form

$$W(\theta) = 1 + a_2 P_2(\cos\theta) + a_4 P_4(\cos\theta)$$

into

$$W(\theta) = 1 + 0.84a_2 P_2(\cos\theta) + 0.54a_4 P_4(\cos\theta).$$

(It has been assumed that the efficiency of the detectors is independent of the point and direction of entry of the  $\gamma$  ray in the crystal. This approximation is reasonable in the present arrangement since the lead collimators between the target and the crystal limit the point of entry of the  $\gamma$  ray to the central 3 inches of the 4-in. diameter crystals.)

A further correction is necessary because of the finite radius of the target. No exact theory has been published for this effect but it can be shown to a first approximation, that a small negative  $P_2(\cos\theta)$  term is introduced in the observed correlation function. For a 1-in. diameter target and detectors 4 inches from the target axis, the  $P_2$  coefficient,  $a_2$  is replaced by  $(a_2 - 0.02)$  for a distribution normalized to unity at  $90^\circ$ . The correction depends upon the square of the radius of the target and is only  $-0.005$  for a  $\frac{1}{2}$ -in. diameter target at 4 in. from the detectors. The inaccuracy resulting from the approximations used in the derivations of the geometric corrections is not considered serious as the full magnitude of the corrections to be applied is in general less than, or of the same order as, the statistical accuracy of the determination of the coefficients in the correlation function.

The equipment was tested, and the corrections checked, by observing the relative coincidence rate at  $180^\circ$  and  $90^\circ$  for cascades in which the correlation functions are well known. The  $\gamma$  ray cascades used were the 1.17- and 1.33-Mev transitions in  $\text{Ni}^{60}$  and the 2.75- and 1.37-Mev transitions in  $\text{Mg}^{24}$  following the  $\beta$  decay of  $\text{Co}^{60}$  and  $\text{Na}^{24}$ , respectively. In both cases the correlation functions are known to be  $W(\theta) = 1 + 0.102P_2(\cos\theta) + 0.009P_4(\cos\theta)$ . The test experiments were made with point sources and with sources 1 inch in diameter and 1 in. long. For the point source the correlation function

expected, after corrections for geometric effects, is

$$W(\theta) = 1 + 0.084P_2(\cos\theta) + 0.005P_4(\cos\theta),$$

which gives the intensity ratio at  $180^\circ$  to that at  $90^\circ$  as

$$I_{180}/I_{90} = 1.14.$$

The corresponding values for the extended source are

$$W(\theta) = 1 + 0.069P_2(\cos\theta) + 0.005P_4(\cos\theta),$$

and

$$I_{180}/I_{90} = 1.11.$$

The observed values, averaged over several separate experiments are

Point source:  $I_{180}/I_{90} = 1.14 \pm 0.01$ .

One-inch diameter source one inch long:  $I_{180}/I_{90} = 1.12 \pm 0.01$ .

These results are in good agreement with the computed values and are taken as confirmation of the corrections applied.

#### IV. MAGNESIUM

The spins of the levels, and the decay scheme of  $\text{Mg}^{25}$  are of considerable interest because of the marked success of Litherland *et al.*<sup>13</sup> in explaining the level structure of  $\text{Mg}^{25}$  and  $\text{Al}^{25}$  in terms of the collective model. It therefore was considered worthwhile to make coinci-

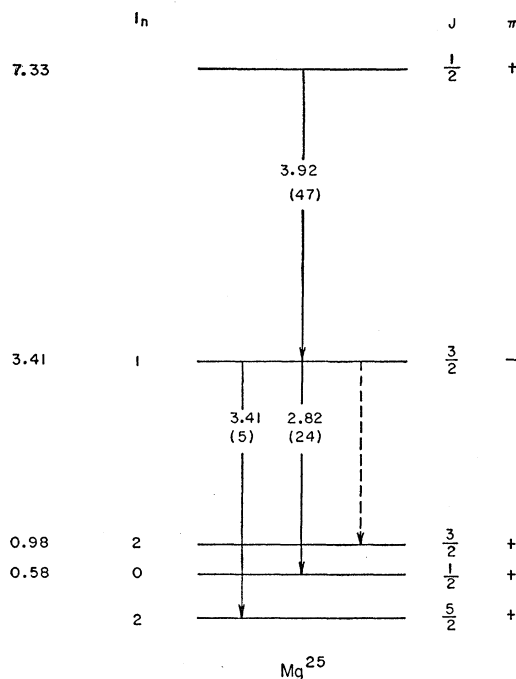


FIG. 4.  $\text{Mg}^{25}$  decay scheme. Only those levels and  $\gamma$  rays relevant to the present experiment are shown. The level energies<sup>20</sup> (in Mev) and the neutron orbital momenta<sup>18</sup> ( $l_n$ ) obtained from  $(d,p)$  measurements are given to the left of the diagram. The  $\gamma$ -ray energies and intensities,<sup>17</sup> in brackets in  $\gamma$  rays per 100 captures in natural magnesium, are shown on the lines representing the transitions.

<sup>13</sup> Litherland, McManus, Paul, Bromley, and Gove, *Can. J. Phys.* **36**, 378 (1958).

dence measurements to confirm some aspects of the decay scheme of  $Mg^{25}$  and angular correlation measurements to confirm the spin of the 3.41-Mev level.

The  $\gamma$ -ray spectrum following thermal-neutron capture in magnesium has been investigated by Kinsey *et al.*,<sup>14</sup> Kinsey and Bartholomew,<sup>15</sup> Braid,<sup>16</sup> and Campion and Bartholomew.<sup>17</sup> Holt and Marsham<sup>18</sup> have measured the proton angular distributions in the  $Mg^{24}(d,p)Mg^{25}$  stripping reaction and conclude that the 3.41-Mev level has negative parity and a spin of  $\frac{1}{2}$  or  $\frac{3}{2}$ . Cox and Williamson<sup>19</sup> conclude from a study of  $(p,\gamma)$  correlations in the  $Mg^{24}(d,p\gamma)Mg^{25}$  reaction that the 3.41-Mev level has a spin of  $\frac{3}{2}$ , a result which was also deduced by Kinsey and Bartholomew<sup>15</sup> from the neutron capture  $\gamma$ -ray decay scheme.

The measurements to be described were made with a sample of pure magnesium metal 1 inch in diameter and 2 inches long. A sample of this size was necessary because of the low neutron cross section of magnesium, *viz.*, 63 mb. Approximately 46% of the neutrons captured in natural magnesium form  $Mg^{25}$  and hence the effective cross section for formation of  $Mg^{25}$  is only 30 mb per atom of natural magnesium. Figure 3 is a typical direct spectrum from one of the detectors. Some of the more prominent  $\gamma$  rays can be identified. Figure 4 shows the relevant parts of the  $Mg^{25}$  decay scheme. Other aspects of the decay scheme are given in the compilation of Endt and Braams.<sup>20</sup> The differential discriminator for the stationary detector was set to include pulses corresponding to an energy loss of 3.7 to 4.2 Mev in the crystal (see Fig. 3). The predominant  $\gamma$  ray accepted from this detector was then the 3.92-Mev primary  $\gamma$  ray to the 3.41-Mev level. The differential discriminator for the movable detector was set to include the energy range 0.1 to 6 Mev. Coincidence measurements were made at angles of  $90^\circ$  and  $180^\circ$  between the two detectors. The spectrum obtained at  $90^\circ$  summed over 14 separate one-hour runs is shown in

TABLE I. Experimental and theoretical values of  $a_2/a_0$  for the 3.92-3.41 and 3.92-2.82 Mev cascades in  $Mg^{25}$ . No  $E1/M2$  mixtures are considered.

Cascade (Mev)	Experimental value of $a_2/a_0$	Theoretical values of $a_2/a_0$	
		Spin of 3.41-Mev level $\frac{1}{2}$	Spin of 3.41-Mev level $\frac{3}{2}$
3.92-3.41	$0.10 \pm 0.05$	0	0.05
3.92-2.82	$0.28 \pm 0.04$	0	0.25

<sup>14</sup> Kinsey, Bartholomew, and Walker, *Phys. Rev.* **83**, 519 (1951).

<sup>15</sup> B. B. Kinsey and G. A. Bartholomew, *Can. J. Phys.* **31**, 901 (1953).

<sup>16</sup> T. H. Braid, *Phys. Rev.* **102**, 1109 (1956).

<sup>17</sup> P. J. Campion and G. A. Bartholomew, *Can. J. Phys.* **35**, 1361 (1957).

<sup>18</sup> J. R. Holt and T. N. Marsham, *Proc. Phys. Soc. London* **A66**, 258 (1953).

<sup>19</sup> S. A. Cox and R. M. Williamson, *Phys. Rev.* **105**, 1799 (1957).

<sup>20</sup> P. M. Endt and C. M. Braams, *Revs. Modern Phys.* **4**, 683 (1957).

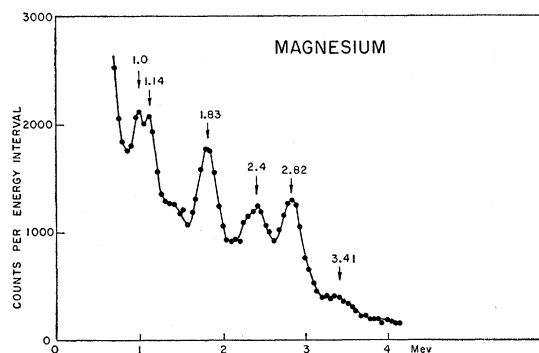


Fig. 5. Typical coincidence spectrum obtained with a magnesium target and discriminator settings as shown in Fig. 3.

Fig. 5. The 2.82-Mev  $\gamma$  ray emitted in the transition between the level at 3.41 Mev and the first excited state of  $Mg^{25}$  at 0.582 Mev can be clearly seen. The 3.41-Mev ground-state  $\gamma$  ray can also be seen but is considerably weaker than the 2.82-Mev  $\gamma$  ray. There is some indication of a  $\gamma$  ray at about 2.4 Mev which is probably due to a transition between the levels at 3.41 and 0.98 Mev. This  $\gamma$  ray is partially masked by the Compton edge of the 2.82-Mev  $\gamma$  ray but it can be seen to be weak compared to the 2.82-Mev line. Other  $\gamma$  rays at about 1.83, 1.14, and 1.0 Mev are transitions in  $Mg^{26}$  and will be discussed later.

The area under the 2.82-Mev peak was computed for the measurements at  $90^\circ$  and  $180^\circ$ . Allowance was made for the contributions from tails of higher energy  $\gamma$  rays under the 2.82-Mev peak. The correlation function was assumed to be of the form  $W(\theta) = a_0 + a_2 P_2(\cos\theta)$ , and the value of  $a_2/a_0$  determined from the results was corrected for distortions due to the finite size of the target and the detectors. A similar analysis was made for the 3.92-3.41 Mev cascade. The results and the theoretical values,<sup>21</sup>  $a_2/a_0$ , for the two possible spins of the 3.41-Mev level are shown in Table I. The results clearly indicate that the spin of the 3.41-Mev level is  $\frac{3}{2}$ .

It is of interest to compare the branching ratio of the 3.41-Mev level with that of the corresponding level in the mirror nucleus  $Al^{25}$ , *viz.*, 3.09 Mev.<sup>13</sup> The latter level emits  $\gamma$  rays to the ground state, first excited state, and second excited state in the ratio 13:78:9. The coincidence spectra shown in Fig. 5 indicates that in  $Mg^{25}$  the transition to the first excited state (2.82-Mev  $\gamma$  ray) is about five times<sup>22</sup> as strong as the transition to the ground state (3.41 Mev) and at least an order of magnitude stronger than the transition to the second excited state (2.42 Mev). This is an illustration of the similarity of the decay schemes of the mirror nuclei.

The  $\gamma$  rays at 1.83, 1.14, and 1.0 Mev (see Fig. 5) are

<sup>21</sup> The 3.92-, 2.82-, and 3.40-Mev  $\gamma$  rays were assumed to be pure electric dipole transitions.

<sup>22</sup> This ratio agrees with that measured with the pair spectrometer.<sup>17</sup> However, the reason for the discrepancy between the intensity of the 3.92-Mev  $\gamma$  ray and the sum of the intensities of  $\gamma$ -rays depopulating the 3.41-Mev level as measured with that instrument is not clear.

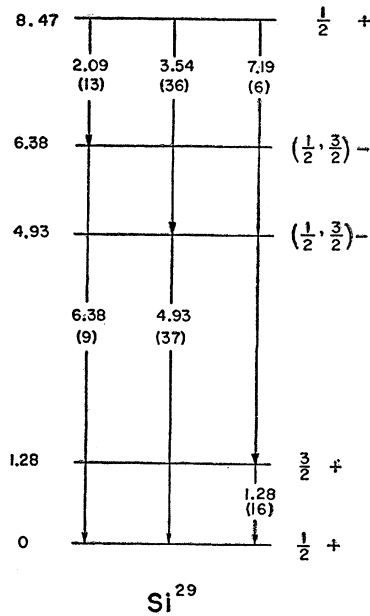


FIG. 6.  $\text{Si}^{29}$  decay scheme. Only those levels and  $\gamma$  rays relevant to the present experiment are shown. The level energies<sup>20</sup> (in Mev) obtained from  $(d,p)$  measurements are given to the left of the diagram. The  $\gamma$  ray intensities<sup>24</sup> in brackets in  $\gamma$  rays per 100 captures in natural silicon and the  $\gamma$  ray energies are shown on the lines representing the transitions.

concluded to be emitted in transitions in  $\text{Mg}^{26}$ . Separate coincidence experiments were made in which the position of the differential discriminator window on the stationary detector was increased in steps of about 0.5 Mev, coincidence spectra being taken at each step. The three  $\gamma$  rays were found to be in coincidence with  $\gamma$  rays of energy at least up to 7 Mev. The binding energy of  $\text{Mg}^{26}$  is 7.33 Mev and hence the  $\gamma$  rays cannot be in  $\text{Mg}^{25}$ . The binding energy of  $\text{Mg}^{26}$  is 11.12 Mev and about 50% of the neutrons captured in natural magnesium form  $\text{Mg}^{26}$ . The 1.83-Mev  $\gamma$  ray is probably emitted in the decay of the first excited state of  $\text{Mg}^{26}$  and the 1.14-Mev  $\gamma$  ray in a transition between the first and second excited states. Similar conclusions were reached by Braid.<sup>16</sup> The 1.0-Mev  $\gamma$  ray may be emitted in a transition between

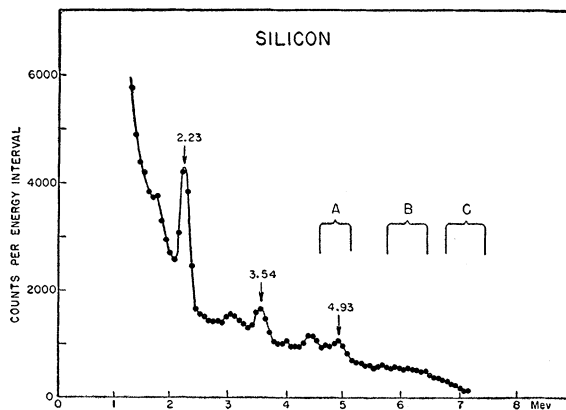


FIG. 7. Typical direct pulse-height spectrum observed using a silicon target. The 2.23-Mev  $\gamma$  ray results from neutron capture in the hydrogen in the Lucite target holder. The intervals A, B, and C show the range of pulse heights accepted by the discriminators of the stationary detector for the coincidence measurements shown in Fig. 8.

the third and second excited states.<sup>23</sup> The fact that these  $\gamma$  rays were seen in coincidence with a window on the stationary detector anywhere between 3 and 7 Mev is some confirmation of the conclusion reached by Campion and Bartholomew<sup>17</sup> that the decay of the capturing state of  $\text{Mg}^{26}$  proceeds mostly by multiple cascade transitions, no single primary  $\gamma$  ray accounting for more than a few percent of the total intensity.

## V. SILICON

The  $\gamma$ -ray spectrum following thermal neutron capture in silicon has been studied by Kinsey *et al.*,<sup>14</sup> Adyasevich *et al.*,<sup>24</sup> and Braid.<sup>16</sup> A convenient summary of the data, including the results of  $(d,p)$  measurements by Van Patter and Buechner<sup>25</sup> and by Holt and Marsham<sup>26</sup> and other pertinent measurements, is given in the compilation of Endt and Braams.<sup>20</sup> Figure 6 contains those parts of the decay scheme relevant to the experiments to be described. Approximately 80% of the neutrons captured in natural silicon form  $\text{Si}^{29}$ . The capture spectrum includes strong primary  $\gamma$  rays to levels at 4.93 and 6.38 Mev. The  $(d,p)$  stripping measurements of Holt and Marsham<sup>26</sup> show these levels to have negative parity and spins of  $\frac{1}{2}$  or  $\frac{3}{2}$ . The purpose of the experiments described below was to determine the spins of these two levels.

The target used for the measurements was approximately 29 g of silicon metal in a Lucite container 2 inches long and 1 inch in diameter. A typical spectrum from one of the detectors is shown in Fig. 7. A few of the

TABLE II. Experimental and theoretical values of  $a_2/a_0$  for the correlation function  $W(\theta) = a_0 + a_2 P_2(\cos\theta)$  for  $(\gamma-\gamma)$  cascades studied in  $\text{Si}^{29}$ . For each transition both the initial state and final state have spin  $\frac{1}{2}$  and even parity. The energy  $E$  in Mev, spin  $J$ , and parity  $\pi$  assumed for the intermediate state are given for each cascade. No  $E1/M2$  mixtures are considered.

Cascade (Mev)	Intermediate state			Theoretical $a_2/a_0$	Experimental $a_2/a_0$
	$E$	$J$	$\pi$		
3.54-4.93	4.93	$\frac{1}{2}$	-	0	$0.25 \pm 0.03$
		$\frac{3}{2}$	-	0.25	
2.09-6.38	6.38	$\frac{1}{2}$	-	0	$0.05 \pm 0.02$
		$\frac{3}{2}$	-	0.25	
7.19-1.28	1.28	$\frac{3}{2}$	+	$A^a$	$0.10 \pm 0.03$

<sup>a</sup>  $A = (1 - x_1^2 + 2\sqrt{3}x_1)(1 - x_2^2 + 2\sqrt{3}x_2) / [4(1 + x_1^2)(1 + x_2^2)]$ , where  $x_1$  and  $x_2$  are the  $E2/M1$  multipole mixture parameters for the 7.19 and 1.28-Mev transitions, respectively.

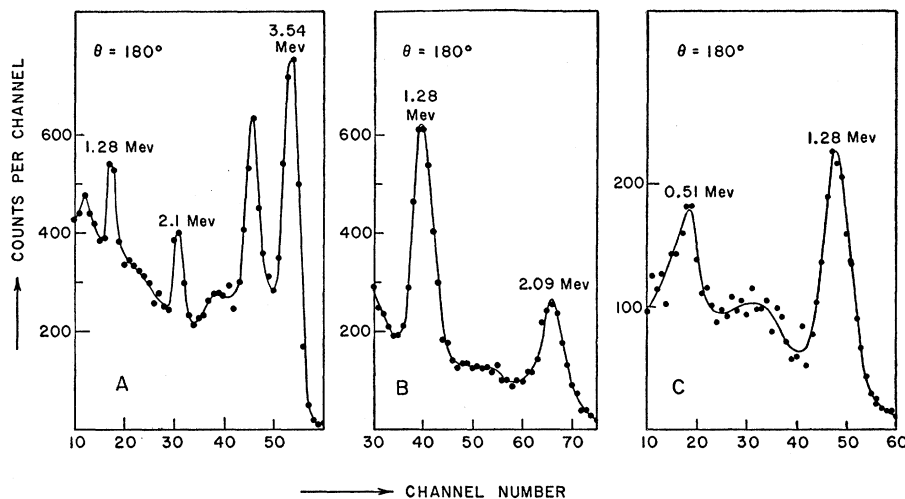
<sup>23</sup> According to May and Foster [Phys. Rev. **90**, 243 (1953)] the 2.97-Mev transition from the 2.97-Mev level is one-sixth as strong as the 1.14-Mev transition. The 2.97-Mev  $\gamma$  ray will contribute to the 2.82-Mev peak in Fig. 5. However, although this radiation could in principle seriously distort the 3.92-2.82 Mev correlation, its intensity is too low to account for all of the observed anisotropy.

<sup>24</sup> Adyasevich, Groshev, and Demidov, *Atomnaya Energ.* **1**, No. 2, 40 (1956).

<sup>25</sup> D. M. Van Patter and W. W. Buechner, Phys. Rev. **87**, 51 (1952).

<sup>26</sup> J. R. Holt and T. N. Marsham, Proc. Phys. Soc. London **A66**, 467 (1953).

FIG. 8. Typical coincidence spectrum obtained with a silicon target and discriminator settings A, B, and C as shown in Fig. 7.



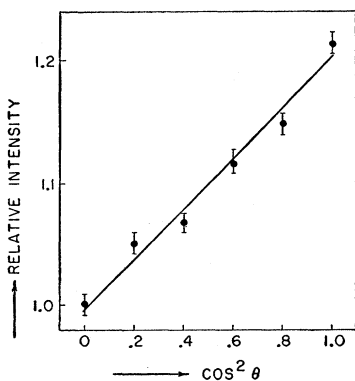
more prominent  $\gamma$  rays can be seen. Coincidence measurements were made with the differential discriminator for the stationary detector set in positions A, B, and C in Fig. 7. The predominant  $\gamma$  rays accepted in these positions were those at 4.93, 6.38, and 7.19 Mev, respectively. Typical coincidence spectra obtained are shown in Fig. 8.

The coincidence measurements for the 3.54-4.93-Mev cascade were made at six different angles between  $90^\circ$  and  $180^\circ$ . The relative counting rate is plotted against  $\cos^2\theta$  in Fig. 9. The results were fitted by least-squares analysis and the coefficient of  $P_2(\cos\theta)$  was corrected for finite-geometry effects.<sup>27</sup> The corrected value of  $a_2/a_0$  was  $0.24 \pm 0.04$ . Correlation measurements for the 2.09-6.38, and 7.19-1.28-Mev cascades and further measurements of the 3.54-4.93-Mev cascade were made at  $90^\circ$  and  $180^\circ$  only. The deduced values of  $a_2/a_0$  after geometric corrections, are given in Table II together with the theoretical values. The 3.54, 4.93, 2.09, and 6.38-Mev  $\gamma$  rays are all  $E1$  and it is assumed that there is no  $M2$  admixture. The 7.19-Mev  $\gamma$  ray is assumed to be an  $E2/M1$  mixture with a multipole mixture parameter,

$x_1 = |S_E|/|S_M|$ , defined by Sharp *et al.*<sup>28</sup> (The phase correction suggested by Huby<sup>29</sup> is included.) The 1.28-Mev  $\gamma$  ray is also assumed to be an  $E2/M1$  mixture with multipole mixture parameter  $x_2$ .

Inspection of Fig. 9 and Table II clearly shows that the 4.93-Mev level is  $\frac{3}{2}^-$ . The small positive coefficient ( $0.05 \pm 0.02$ ) for the 2.09-6.38 Mev cascade is smaller than the value expected for a spin of  $\frac{3}{2}$  for the 6.38-Mev

FIG. 9. Observed correlation between the 3.54- and 4.93-Mev  $\gamma$  rays in  $\text{Si}^{29}$  uncorrected for finite size of the target and detectors. The line shows a least-squares fit to the experimental points. The correlation function, after corrections for finite size of the target and detectors, is  $W(\theta) = 1 + (0.24 \pm 0.04)P_2(\cos\theta)$ .



<sup>27</sup> This measurement was made with the detectors nearer to the target than was used for the other measurements reported here.

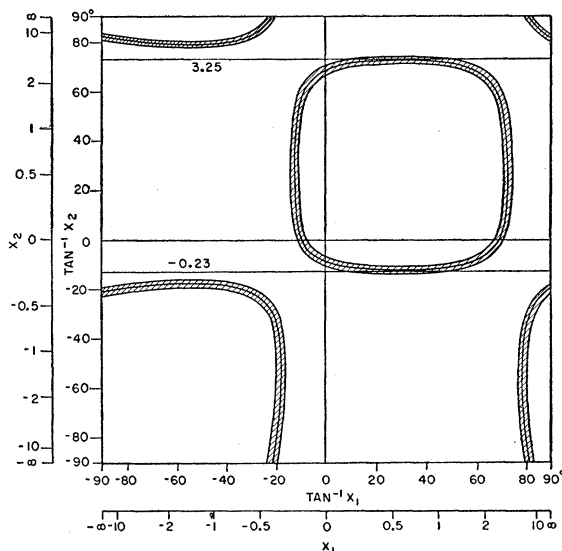


FIG. 10. Contour plot of the theoretical value of  $a_2/a_0$  in the correlation function for the 7.19-1.28 Mev cascade in  $\text{Si}^{29}$ .  $x_1$  and  $x_2$  are the  $E2/M1$  multipole mixture parameters for the 7.19- and 1.28-Mev  $\gamma$  rays, respectively. (The multipole mixture parameters are taken from Sharp *et al.*<sup>28</sup> The Huby<sup>29</sup> correction is included.) The observed value of  $a_2/a_0$  is  $0.10 \pm 0.03$  and the cross hatched area shows the region between  $a_2/a_0$  of 0.07 and 0.13. Bromley *et al.*<sup>30</sup> have determined the value of  $x_2$  to be  $-0.23$  or  $3.25$ . Intersection of their values with the crosshatched region indicate possible values of  $x_1$  between  $+0.27$  and  $+1.2$  approximately.

<sup>28</sup> Sharp, Kennedy, Sears, and Hoyle, Chalk River Report CRT-556, 1954 (unpublished).

<sup>29</sup> R. Huby, Proc. Phys. Soc. London A67, 1103 (1954).

level, *viz.*, 0.25. The level is concluded to be  $\frac{1}{2}-$  and the small positive term is believed to be due to a small contribution from other cascades. The 7.19–1.28-Mev correlation indicates that one, or both, of the  $\gamma$  rays has an  $E2$  component. Figure 10 is a contour plot of the theoretical values of  $a_2/a_0$  for a  $\frac{1}{2}+$  to  $\frac{3}{2}+$  to  $\frac{1}{2}+$  transition for all possible values of  $x_1$  and  $x_2$  from  $-\infty$  to  $+\infty$ . Contours for  $a_2/a_0=0.07, 0.10,$  and  $0.13$  are shown. The experimentally observed value was  $0.10 \pm 0.03$ . Bromley *et al.*<sup>30</sup> have measured the multipole mixture parameter for the 1.28-Mev  $\gamma$  ray. Their values are  $x_2=-0.23$  or  $3.25$ . These values are shown in Fig. 10. The intersections of their values with the shaded region in Fig. 10 indicate that the mixture parameter for the 7.18-Mev  $\gamma$  ray falls between  $+0.27$  and  $+1.2$  approximately.

Bromley *et al.*<sup>31</sup> have applied the collective model to the nucleus  $\text{Si}^{29}$ . The results of these authors are consistent with an oblate shape for the nucleus and a spheroidicity,  $\delta$ , of  $-0.15$ .  $\delta=R/R_0$  where  $R_0$  is the mean radius and  $R$  is the difference between the major and minor semiaxes.<sup>32</sup> The most probable Nilsson orbits

which correspond to the 4.93 Mev ( $\frac{3}{2}-$ ) and 6.23 Mev ( $\frac{1}{2}-$ ) levels would appear to be orbits 16 and 17. These are chosen because they have a strong contribution from the  $p$  shell at a distortion of  $\delta=-0.15$  and hence can account for the strong dipole  $\gamma$  rays to the levels and the large reduced widths, of the proton groups (see Fujimoto *et al.*<sup>33</sup>) to these levels in the  $\text{Si}^{28}(d,p)\text{Si}^{29}$  reaction. In addition the computed energy difference between these two orbits is about equal to the observed value.

## VI. PHOSPHORUS

The  $\gamma$  rays following thermal neutron capture in phosphorus have been investigated by Kinsey *et al.*<sup>34,35</sup> and by Braid.<sup>16</sup> Phosphorus has only one stable isotope,  $\text{P}^{31}$ , and hence all  $\gamma$  rays observed belong to the decay of  $\text{P}^{32}$ . The level structure of this nucleus has been investigated using the  $\text{P}^{31}(d,p)\text{P}^{32}$  reaction by Van Patter *et al.*<sup>36</sup> and by Dalton *et al.*<sup>37</sup> The latter authors have made proton angular distribution measurements and have determined the parities, and placed limits on the spins, of some of the levels. The ground state spin of  $\text{P}^{32}$  has been measured to be 1 by Feher *et al.*<sup>38</sup> The proton stripping pattern to the ground-state doublet (the first excited state is at 0.08 Mev) shows that both levels are of positive parity and the relative yield<sup>39</sup> to the two levels indicates that the probable spin of the first excited state is 2. The ground-state spin and parity of  $\text{P}^{31}$  is  $\frac{1}{2}+$  and hence thermal neutron capture can form compound states in  $\text{P}^{32}$  of  $0+$  or  $1+$ . The relative contributions of the two possible spin states are not known. A review of current knowledge of the neutron capture  $\gamma$  ray decay scheme of  $\text{P}^{32}$  is given in the compilation of Endt and Braams.<sup>20</sup> Figure 11 shows the transitions relevant to the experiments described below.

The sample used was approximately 23 g of red phosphorus in a Lucite container one inch in diameter and two inches long. Figure 12 shows the direct spectrum from one of the detectors. Some of the more prominent  $\gamma$  rays observed by Kinsey *et al.*<sup>34</sup> and by Braid<sup>16</sup> are just resolved. Coincidence spectra were taken for three different positions of the window of the differential discriminator. These are shown as *A*, *B*, and *C* in Fig. 12. Position *A* included the 6.76-Mev primary  $\gamma$  ray to the 1.15-Mev level, position *B* the 4.68-Mev primary  $\gamma$  ray to the 3.26-Mev level and position *C* accepted the 0.08-Mev  $\gamma$  ray from the first excited state to the ground state. Figures 13(A), 13(B), and 13(C) show typical coincidence spectra obtained with these discriminator

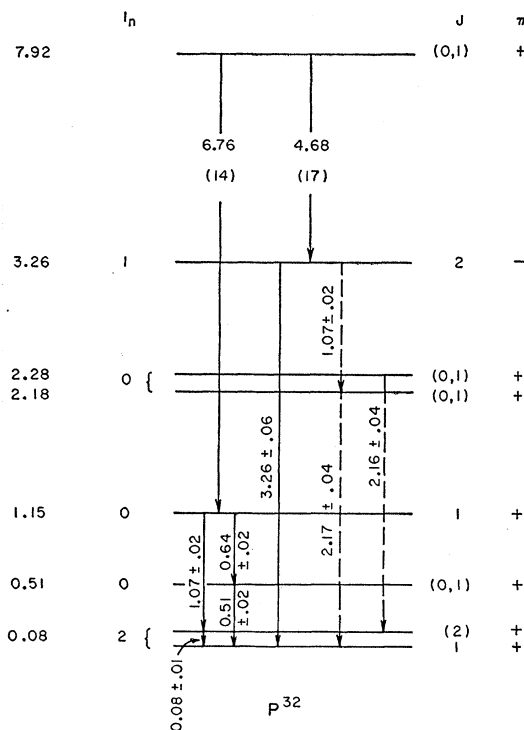


FIG. 11.  $\text{P}^{32}$  decay scheme. Only those levels and  $\gamma$  rays relevant to the present experiment are shown. The level energies<sup>20</sup> (in Mev) and the neutron orbital momenta<sup>26</sup> ( $l_n$ ) obtained from  $(d,p)$  measurements are given to the left of the diagram. The intensities<sup>39</sup> (in brackets in  $\gamma$  rays per 100 captures in phosphorus) and energies<sup>34</sup> for the primary  $\gamma$  rays are shown on the lines representing the transitions. The energies shown for the other  $\gamma$  rays are taken from the present work.

<sup>30</sup> Bromley, Gove, Paul, Litherland, and Almqvist, *Can. J. Phys.* **35**, 1042 (1957).

<sup>31</sup> Bromley, Gove, and Litherland, *Can. J. Phys.* **35**, 1057 (1957).

<sup>32</sup> S. G. Nilsson, *Kgl. Danske Videnskab. Selskab, Mat.-fys. Medd.* **29**, No. 16 (1955).

<sup>33</sup> Fujimoto, Kikuchi, and Yoshida, *Progr. Theoret. Phys. Kyoto* **11**, 264 (1954).

<sup>34</sup> Kinsey, Bartholomew, and Walker, *Phys. Rev.* **85**, 1012 (1952).

<sup>35</sup> Revised intensities are given in a compilation by G. A. Bartholomew and L. A. Higgs, Atomic Energy of Canada Limited, Chalk River Report AECL-669, 1958 (unpublished).

<sup>36</sup> Van Patter, Endt, Sperduto, and Buechner, *Phys. Rev.* **86**, 502 (1952).

<sup>37</sup> Dalton, Hinds, and Parry, *Proc. Phys. Soc. London* **A70**, 586 (1957).

<sup>38</sup> Feher, Fuller, and Gene, *Phys. Rev.* **107**, 1462 (1957).

<sup>39</sup> H. A. Enge, *Phys. Rev.* **94**, 730 (1954); W. C. Parkinson, *Phys. Rev.* **110**, 485 (1958).

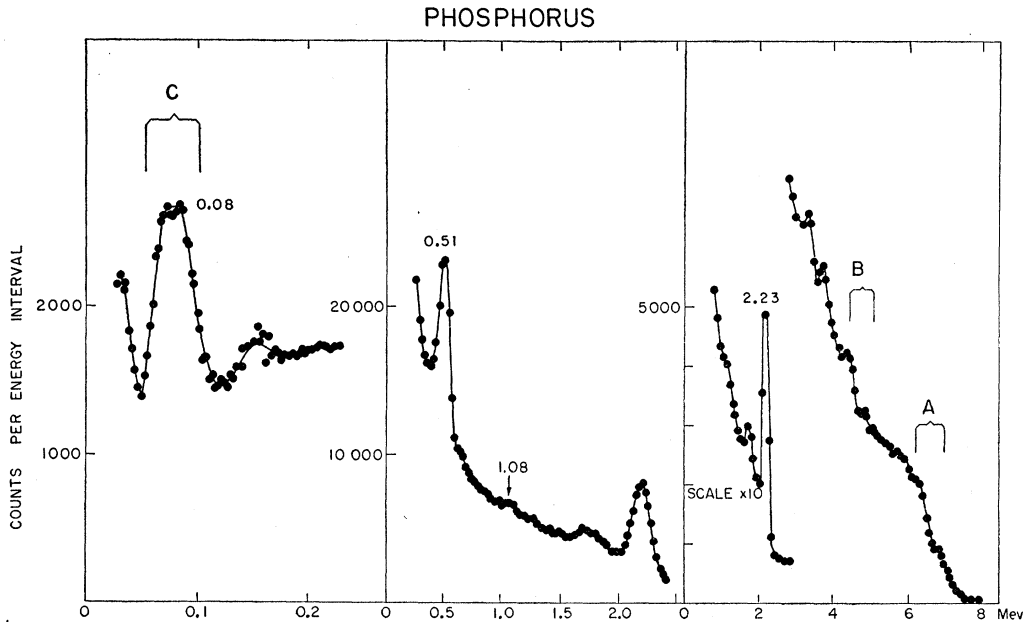


FIG. 12. Typical direct pulse height spectrum observed with a phosphorus target. Part of the peak at 2.23 Mev results from neutron capture in the hydrogen in the Lucite target support. Annihilation radiation contributes to the peak at 0.51 Mev. The intervals A, B, and C show the range of pulse heights accepted by the discriminators of the stationary detector for the coincidence measurements shown in Fig. 13.

settings. The spectrum in coincidence with the 6.76-Mev  $\gamma$  ray, see Fig. 13(A), contains peaks at  $1.07 \pm 0.02$ ,  $0.64 \pm 0.02$ ,  $0.51 \pm 0.02$ ,<sup>40</sup> and  $0.08 \pm 0.01$  Mev. The positions of these  $\gamma$ -rays in the decay scheme are shown in Fig. 11. There is no evidence for a  $\gamma$  ray of 1.15 Mev which might be emitted in a transition between the 1.15-Mev level and the ground state. If this  $\gamma$  ray exists it accounts

for less than 10% of the decays from the 1.15-Mev level. The spectrum in coincidence with the 4.68-Mev  $\gamma$  ray [see Fig. 13(B)] shows peaks at  $3.26 \pm 0.06$ ,  $2.17 \pm 0.04$ ,  $1.07 \pm 0.02$ , and  $0.51 \pm 0.02$  Mev. The 3.26-Mev  $\gamma$  ray is the ground state transition from the 3.26-Mev level. The  $\gamma$  rays at 2.17 and 1.07 Mev are probably due to a double cascade from the 3.26-Mev level to the ground

TABLE III. Theoretical and experimental values of  $a_2/a_0$  for the correlation function  $W(\theta) = a_0 + a_2 P_2(\cos\theta)$  for ( $\gamma = \gamma$ ) cascades studied in  $P^{32}$ . The theoretical values shown are calculated on the assumption that all  $\gamma$  rays are pure dipole radiation. This is a reasonable assumption if the radiation is between states of different parity. The energy  $E$  in Mev, spin  $J$ , and parity  $\pi$ , are given for the initial, intermediate, and final states. Only spin values consistent with the ( $d, p$ ) measurements of Dalton *et al.*<sup>a</sup> are considered. Both possible spins for the capturing state are included.

Cascade (Mev)	Initial state			Intermediate state			Final state			Theoretical $a_2/a_0$	Experimental $a_2/a_0$
	$E$	$J$	$\pi$	$E$	$J$	$\pi$	$E$	$J$	$\pi$		
4.68-3.26	7.92	0	+	3.26	1	-	0	1	+	-0.25	+0.19±0.03
		1	+		1	-		1	+	+0.125	
		1	+		2	-		1	+	+0.175	
6.76-1.07	7.92	0	+	1.15	1	+	0.08	2	+	+0.05	+0.10±0.03
		1	+		1	+		2	+	-0.025	
		0	+		1	+		1	+	-0.25	
		1	+		1	+		1	+	+0.125	
6.76-0.64	7.92	0	+	1.15	1	+	0.51	0	+	+0.5	-0.16±0.05
		1	+		1	+		0	+	-0.25	
		0	+		1	+		1	+	-0.25	
		1	+		1	+		1	+	+0.125	
1.07-0.08	1.15	1	+	0.08	1	+	0	1	+	+0.125	+0.09±0.04
		1	+		2	+		1	+	+0.175	

<sup>a</sup> See reference 37.

<sup>40</sup> Part of this radiation is probably due to annihilation radiation from the other detector. It cannot all be ascribed to this cause however, since the presence of the 0.64-Mev  $\gamma$  ray implies the presence of either a 0.51 or a 0.44-Mev  $\gamma$  ray (Fig. 11) and there is no evidence in Fig. 13(A) for a peak at 0.44 Mev.

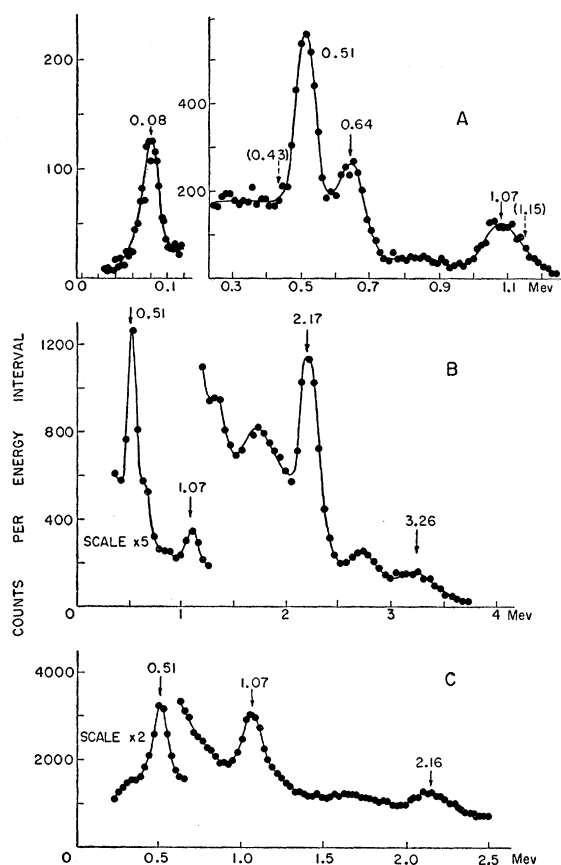


Fig. 13. Typical coincidence spectra at a detector angle of  $90^\circ$  obtained using a phosphorus target and discriminator settings shown as *A*, *B*, and *C* in Fig. 12. *A* shows  $\gamma$  rays in coincidence with the 6.76-Mev  $\gamma$  ray, *B* shows those in coincidence with the 4.68-Mev  $\gamma$  ray, and *C* shows those in coincidence with the 0.08-Mev  $\gamma$  ray. See Fig. 11 for the probable positions of these radiations in the decay scheme.

state via the level at 2.18 Mev. The spectrum in coincidence with the 0.08-Mev  $\gamma$  ray<sup>41</sup> [see Fig. 13(C)] contains peaks at  $2.16 \pm 0.04$ ,  $1.07 \pm 0.02$ , and  $0.51 \pm 0.02$  Mev. The peak at 1.07 Mev confirms that the level at 1.15-Mev decays in part by a cascade transition through the first excited state. The peak at  $2.16 \pm 0.04$  Mev is probably due to a cascade transition from the level at 2.28 Mev but may be due in part to a cascade from the level at 2.18 Mev.

The coincidence measurements described above were made with angles of  $90^\circ$  and  $180^\circ$  between the counters. The measurements were repeated many times and the relative counting rate at the two angles was determined for the following cascades: 4.68–3.26, 6.76–1.07, 1.07–0.08, and 6.76–0.64 Mev. The experimental values of  $a_2/a_0$  are given in Table III together with the theoretical values on the assumption that all  $\gamma$  rays are pure dipole radiation. This assumption is nearly certain to be correct when the transition is between levels of opposite

<sup>41</sup> The observation of coincidences involving the 0.08-Mev  $\gamma$  ray shows that the mean life of the first excited state is  $\leq 4 \times 10^{-8}$  sec. This is consistent with the conclusion that the 0.08-Mev  $\gamma$  ray is *M1* and not pure *E2*.

parity, but can be incorrect when the levels have the same parity since some electric quadrupole transitions may compete with magnetic dipole transitions. In Table III all possible spin values compatible with the (*d,p*) stripping measurements of Dalton *et al.*<sup>37</sup> are considered. All of the correlations measured were significantly anisotropic and hence one may definitely conclude, without any assumption concerning the forms of the radiations, that the spins of the levels at 3.26, 1.15, and 0.08 Mev are not zero. The stripping pattern to the 1.15-Mev level shows that the level has positive parity and a spin of 0 or 1. We therefore conclude the level is  $1+$ . As the proportion of spin 1 and spin 0 responsible for neutron capture by  $P^{31}$  is not known, those cascades involving the capturing state listed in Table III are shown with both possibilities (transitions from spin 0 to spin 2 are excluded as only dipole radiations are considered). The states of different spin cannot interfere in *s*-wave capture and if both spin states are formed the observed correlation function should fall between the two listed correlation functions. The 4.68–3.26 Mev cascade consists of two electric dipole  $\gamma$  rays and no quadrupole mixture is likely. If the 3.26-Mev level were of spin 1, the correlation function should lie between  $+0.125$  and  $-0.25$ . The observed value,  $0.19 \pm 0.03$ , is outside these limits but is consistent with the value predicted for a

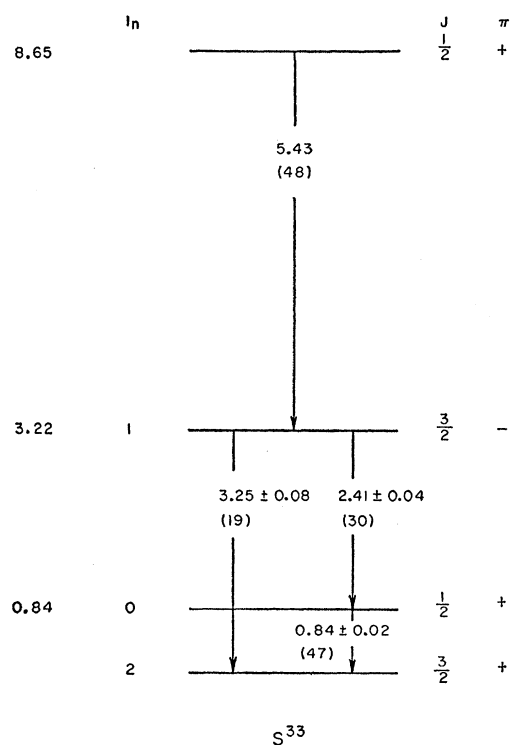


Fig. 14.  $S^{33}$  decay scheme. Only those levels and  $\gamma$  rays relevant to the present experiment are shown. The level energies<sup>30</sup> (in Mev) and neutron orbital momenta<sup>26</sup> ( $l_n$ ) obtained from (*d,p*) measurements are given to the left of the diagram. The intensities,<sup>43</sup> in brackets, in  $\gamma$  rays per 100 captures in sulfur and the energies of the  $\gamma$  rays are shown on the lines representing the transitions. The energies of all but the primary  $\gamma$  ray are taken from the present work.

spin of 2 for the 3.26-Mev level. The 3.26-Mev level is concluded to be 2-. Thus only the spin 1 part of the "capturing state" will contribute to the 4.68-Mev  $\gamma$  ray and at least 17% of the capture must proceed through a compound state of spin 1.

The four  $\gamma$  rays involved in the three other cascades considered are between states of the same parity and may be  $E2/M1$  mixtures. With the data available no unique solution can be found for the spins of the levels involved. If the spin of the 0.08-Mev level<sup>39</sup> is 2, the 1.07-0.08 Mev correlation shows that either the 1.07- or 0.08-Mev  $\gamma$  ray has an appreciable  $E2$  component. If the spin of the 0.08-Mev level is 1, all of the observed results can be fitted with pure  $M1$  radiation. Then the 6.76-1.07 and 6.76-0.64 Mev correlations can be fitted by assuming that the 6.76-Mev transition is approximately 90% a 1+ to 1+ transition and 10% a 0+ to 1+ transition, and that the spin of the 0.51-Mev level is 0. The solutions just considered were chosen to illustrate that no unique spin assignment for the 0.08-Mev state can be determined from our data alone.

VII. SULFUR

The  $\gamma$  spectrum following thermal neutron capture in sulfur has been investigated by Kinsey *et al.*,<sup>34</sup> Kinsey and Bartholomew,<sup>42</sup> Groshev *et al.*,<sup>43</sup> and Braid.<sup>16</sup> All  $\gamma$  rays are presumed to be emitted in the decay of  $S^{33}$ . The levels of this nucleus have been investigated by the  $S^{32}(d,p)S^{33}$  reaction by Paris and Endt<sup>44</sup> and by Holt and Marsham.<sup>26</sup> A decay scheme for  $S^{33}$  is given in the compilation of Endt and Braams,<sup>20</sup> and Fig. 14 shows the energy levels relevant to the work described here. The level at 3.22 Mev, which is fed strongly following neutron capture, is known from the  $(d,p)$  stripping measurements of Holt and Marsham<sup>26</sup> to have negative parity and a spin of  $\frac{1}{2}$  or  $\frac{3}{2}$ . Trumpy<sup>3</sup> has measured the circular polarization of the 5.43-Mev primary  $\gamma$  ray to the 3.22-Mev level following capture of polarized thermal neutrons and concludes that the level is  $\frac{3}{2}$ -. The purpose of the present experiment was to confirm that assignment.

A sample of approximately 7 g of pure sulfur in a

TABLE IV. Theoretical and experimental values of  $a_2/a_0$  for the correlation function  $W(\theta) = a_0 + a_2P_2(\cos\theta)$  for the  $(\gamma$ - $\gamma)$  cascades studied in  $S^{33}$ . No  $E1/M2$  mixtures are considered.

Cascade (Mev)	Theoretical value of $a_2/a_0$		Experimental value of $a_2/a_0$
	Spin of 3.22-Mev level $\frac{1}{2}$	Spin of 3.22-Mev level $\frac{3}{2}$	
5.43-3.25	0	-0.2	$-0.15 \pm 0.04$
5.43-2.41	0	+0.25	$+0.26 \pm 0.04$
5.43-0.84	0	0	$0 \pm 0.03$

<sup>42</sup> B. B. Kinsey and G. A. Bartholomew, *Phys. Rev.* **93**, 1260 (1954).

<sup>43</sup> Groshev, Adyasevich, and Demidov, *Proceedings of the International Conference on the Peaceful Uses of Atomic Energy, Geneva, 1955* (Columbia University Press, New York, 1956), Vol. 2, p. 39.

<sup>44</sup> Paris, Buechner, and Endt, *Phys. Rev.* **100**, 1317 (1955). See also Endt and Braams,<sup>20</sup>

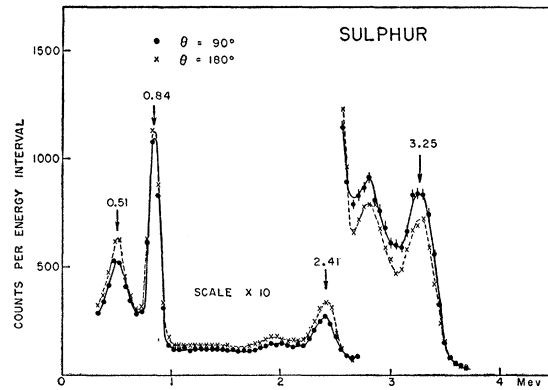


Fig. 15. Spectrum from sulfur target in coincidence with pulses in range 5.1 to 5.7 Mev. Spectra for 90° and 180° are for equal counting periods.

thin Lucite container 1 inch in diameter and 1 inch long was used for the measurements. The differential discriminator for the stationary detector was set to accept pulses corresponding to an energy loss of 5.1 to 5.7 Mev in the crystal. Typical coincidence spectra obtained for 90° and 180° between the detectors are shown in Fig. 15. Peaks can be seen corresponding to  $\gamma$  rays of  $3.25 \pm 0.08$ ,  $2.41 \pm 0.04$ ,  $0.84 \pm 0.02$ , and  $0.51 \pm 0.02$  Mev. The position of these  $\gamma$  rays in the decay scheme is shown in Fig. 14. Table IV gives the deduced  $a_2/a_0$  coefficient, corrected for finite geometry, for the 5.43-3.25, 5.43-2.41, and 5.43-0.84 Mev cascades. The theoretical values are also given for the two possible spin values for the 3.22-Mev level. All  $\gamma$  rays are presumed to be pure dipole radiation. Inspection of Table IV clearly shows that the 3.22-Mev level has spin  $\frac{3}{2}$ . Our measurements thus confirm the assignment of Trumpy.<sup>3</sup>

VIII. CONCLUSIONS

The measurement of angular correlations between neutron capture  $\gamma$  rays has resulted in the determination or verification of the spins of one or two levels for each of the four elements studied. Specifically the results are:  $Mg^{25}$ , 3.41-Mev level  $\frac{3}{2}$ ;  $Si^{29}$ , 4.93-Mev level  $\frac{3}{2}$ ; 6.38-Mev level  $\frac{1}{2}$ ;  $P^{32}$ , 1.15-Mev level 1; 3.26-Mev level 2; and  $S^{33}$ , 3.22-Mev level  $\frac{3}{2}$ . A similar yield of spin determinations per nucleus was obtained by Trumpy<sup>3</sup> for elements near iron. With the  $\gamma$ -ray detectors now available, the present technique clearly can be extended to measurement of triple correlations and polarization direction correlations between neutron capture  $\gamma$  rays in favorable cases. However, in order for these methods to be used more generally in more complex spectra, detectors with comparable efficiency but with much better resolution are obviously required.

IX. ACKNOWLEDGMENTS

The authors wish to thank Mr. D. Stairs for his assistance in taking data for these experiments. The interest and help of Dr. A. E. Litherland, Dr. H. E. Gove, Dr. E. B. Paul, Dr. H. Carmichael, and Dr. L. G. Elliott are also gratefully acknowledged.